# Excitonic collective modes in Weyl semimetals

N. S. Srivatsa[1,2,*] and R. Ganesh[1,†]

[1]*The Institute of Mathematical Sciences, HBNI, C I T Campus, Chennai 600 113, India*

[2]*Max Planck Institute for the Physics of Complex Systems, Nöthnitzer Str. 38, 01187 Dresden, Germany*

(Received 20 August 2018; published 23 October 2018)

Weyl semimetals are three-dimensional analogs of graphene with pointlike Fermi surfaces. Their linear electronic dispersion leads to a window in the particle-hole excitation spectrum which allows for undamped propagation of collective excitations. We argue that interactions in Weyl semimetals generically lead to well-defined exciton modes. However, using a minimal model for interactions, we show that the exciton binding energy is exponentially small for weak interactions. This is due to effective two-dimensional character in the space of particle-hole pairs that are available for bound-state formation. This is ultimately a consequence of linear electronic dispersion in three dimensions. Nevertheless, intermediate interaction strengths can lead to sharp excitonic resonances. We demonstrate this in a model Weyl semimetal with broken time-reversal symmetry and Hubbard interactions. Using generalized random phase approximation analysis, we show that excitonic modes here carry spin. Excitons in Weyl semimetals have evoked interest as their condensation could lead to an axionic charge-density-wave order. However, we find that the leading instability corresponds to intravalley spin density wave order which shifts the Weyl points without opening a gap. Our results suggest interesting directions for experimental studies of three-dimensional Dirac systems.

DOI: 10.1103/PhysRevB.98.165133

## I. INTRODUCTION

Dirac systems such as graphene [1], Weyl semimetals [2,3], and Dirac semimetals [4] are of great interest due to their pointlike Fermi surfaces and conical dispersions. The effects of electron-electron interactions in these systems are especially interesting [5] with studies focusing on quasiparticle character, ordering instabilities, etc. A particularly elegant feature was pointed out by Jafari and Baskaran in the context of graphene [6,7]. They argued that conical dispersion leads to a windowlike structure in the particle-hole continuum within which excitonic modes can propagate. In this paper, we extend this notion to three-dimensional Weyl semimetals. We show that they generically host undamped collective excitations. Furthermore, these modes may be imbued with spin due to inherent spin-orbit coupling.

The suitability of Weyl semimetals for hosting exciton collective modes stems from their linear dispersion. This is illustrated in Fig. 1(a) for a simple Weyl semimetal. It has two Weyl points which occur at incommensurate wave vectors separated by **Q**. Low-energy quasiparticle excitations can occur in either valley. The corresponding particle-hole continuum is shown schematically in Fig. 1(b). At low energies, it consists of two cones centered at momentum zero and **Q**, corresponding to intravalley and intervalley particle-hole excitations, respectively. This continuum is very different from that of a conventional metal, say with a spherical Fermi surface. In the latter, low-energy excitations near the Fermi surface form a swathelike particle-hole continuum, extending to zero energy over a wide range of momentum values. In contrast, the Weyl semimetal possesses a window structure which can host collective excitations as shown in Fig. 1(b). Such a collective mode will remain undamped as it cannot decay into particle-hole pairs while conserving energy and momentum.

The impact of electron interactions on the stability of a Weyl semimetal is a question of considerable interest. Due to the vanishing density of states at the Fermi level, it is readily seen that weak interactions cannot bring about instabilities. However, a sufficiently strong interaction will lead to ordering instabilities [8–10]. A straightforward comparison can be made with the honeycomb lattice Hubbard model, which develops an antiferromagnetic instability at a critical interaction strength [11]. In Weyl semimetals, an elegant possibility is an instability to an "axionic insulator" [12–14]. This emerges as a natural intervalley "mass" term that opens an electronic gap. The physics of this transition and the associated soft modes is of great interest. In particular, it has been argued that low-energy behavior in the vicinity of this transition exhibits emergent supersymmetry [15]. This prompts the following question: Is there a microscopic model with a tunable parameter that can realize axion condensation? We study a Hubbard model which is the simplest plausible microscopic paradigm. However, we find that the Hubbard interaction merely shifts the Weyl points and does not open a gap.

The remainder of this paper is structured as follows. In Sec. II, we outline the generalized random phase approximation (GRPA) formalism that we use to find collective excitations. In Sec. III, we consider a simplistic model for interactions in a Weyl semimetal which allows for an analytic calculation of the collective mode spectrum. We show

*srivatsa@pks.mpg.de

†ganesh@imsc.res.in

 

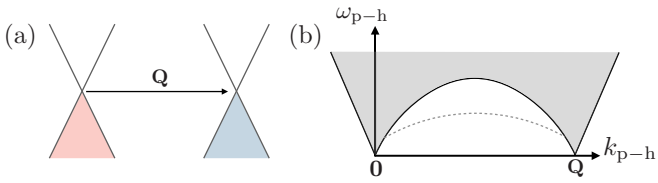


FIG. 1. (a) Dispersion in a minimal Weyl semimetal with two valleys separated by momentum $\mathbf{Q}$. (b) The corresponding particle-hole continuum. Low-energy particle-hole excitations can either be intravalley ($\mathbf{k}_{\text{p-h}} \sim \mathbf{0}$) or intervalley ($\mathbf{k}_{\text{p-h}} \sim \mathbf{Q}$). The resulting window structure allows for the propagation of an undamped collective mode, schematically shown as a dashed line.

that linear electronic dispersion leads to an effectively two-dimensional phase space for exciton formation. Next, in Sec. IV, we consider Hubbard interactions in a model Weyl semimetal. We show that excitonic modes occur with intravalley as well as intervalley character. Section V discusses exciton properties such as binding energy and spinful character. It demonstrates that exciton condensation leads to magnetic order. We conclude with a summary and discussion in Sec. VI.

## II. GENERALIZED RANDOM PHASE APPROXIMATION

We first describe the GRPA scheme [16] for finding collective excitations in general terms. In the following sections, we apply this formalism to models with increasing level of detail. This is a weak coupling approach where we begin with a noninteracting Hamiltonian, denoted by $\mathcal{H}_{KE}$. We calculate its susceptibility to various orders. We then include interaction terms which modify this "bare" susceptibility. Finally, we identify divergences in the renormalized GRPA susceptibility as collective mode resonances. This approach is equivalent to summation over ladder diagrams (e.g., compare Refs. [17,18]), the Bethe-Salpeter equation [19,20], and equations-of-motion approaches [21]. It has been shown to work well even in the strong coupling limit where it provides good agreement with the appropriate spin-wave expansion [18,22].

Starting with an appropriate noninteracting Hamiltonian $\mathcal{H}_{KE}$, we consider various ordering tendencies represented by fermionic bilinears, e.g., $\hat{\mathbf{S}}_{\mathbf{q}} \equiv \sum_{\mathbf{k}} c^{\dagger}_{\mathbf{k}+\mathbf{q},\mu}\sigma_{\mu,\nu}c_{\mathbf{k},\nu}$ for spin-density-wave order at momentum $\mathbf{q}$. We collect all such relevant bilinears into an array $\hat{O}(\mathbf{q})$. Assuming fictitious fields that couple to these bilinears, we have

$$\mathcal{H} = \mathcal{H}_{KE} - \frac{1}{N}\sum_{\mathbf{q}} h_{\beta}(q,t)\hat{O}^{\dagger}_{\beta}(\mathbf{q}), \tag{1}$$

where $N$ is the number of sites in the system. Throughout this paper, repeated indices are to be summed over. Within linear response, these fields induce expectation values given by

$$\langle \hat{O}_{\alpha}\rangle(\mathbf{q},t) = \int_{-\infty}^{\infty} dt' \chi^{0}_{\alpha\beta}(\mathbf{q},t-t')h_{\beta}(\mathbf{q},t'). \tag{2}$$

The bare susceptibility matrix $\chi^0$ is computed using the spectrum of $\mathcal{H}_{KE}$ (assuming zero temperature),

$$\chi^{0}_{\alpha\beta}(\mathbf{q},t-t') = i\frac{\theta(t-t')}{N}\langle[\hat{O}_{\alpha}(\mathbf{q},t),\hat{O}^{\dagger}_{\beta}(\mathbf{q},t')]\rangle_{\mathcal{H}_{KE}}. \tag{3}$$

This can be directly evaluated in frequency space to give $\chi^0_{\alpha\beta}(\mathbf{q},\omega)$, which takes a form similar to the Lindhard function. We have $\langle \hat{O}_{\beta}\rangle(\mathbf{q},\omega) = \chi^0_{\alpha\beta}(\mathbf{q},\omega)h_{\beta}(\mathbf{q},\omega)$.

We next consider interactions represented by two particle processes, denoted by $\mathcal{H}_{\text{int}}$. In the GRPA scheme, this is quadratically decoupled so as to renormalize the effective fields in Eq. (1). We have

$$\mathcal{H}_{\text{int}} \longrightarrow \frac{g}{N}\langle \hat{O}_{\alpha}\rangle \cdot D_{\alpha\beta} \cdot \hat{O}^{\dagger}_{\beta}, \tag{4}$$

where $g$ is the interaction strength and $D_{\alpha\beta}$ is a coupling matrix. The expectation values $\langle \hat{O}_{\alpha}\rangle$ can depend on space and time. These quadratically decomposed terms renormalize the coupling fields in Eq. (1), leading to

$$\langle \hat{O}_{\alpha}\rangle = \chi^{0}_{\alpha\beta}(h_{\beta} - gD_{\tau\beta}\langle \hat{O}_{\tau}\rangle). \tag{5}$$

Upon rearranging the above equation, we arrive at an expression for the expectation value of the induced order

$$\langle \hat{O}_{\alpha}\rangle(\mathbf{q},\omega) = \chi^{\text{GRPA}}_{\alpha\beta}(\mathbf{q},\omega)h_{\beta}(\mathbf{q},\omega), \tag{6}$$

where

$$\chi^{\text{GRPA}}_{\alpha\beta} = [(1+g\chi^{0}D)^{-1}\chi^{0}]_{\alpha\beta}. \tag{7}$$

This gives the GRPA susceptibility matrix at momentum $\mathbf{q}$ and frequency $\omega$. We have suppressed $(\mathbf{q},\omega)$ arguments of $\chi^0$ and $\chi^{\text{GRPA}}$ for simplicity. Operationally, we first evaluate $\chi^0$, numerically if necessary. We then seek $(\mathbf{q},\omega)$ where $(1+g\chi^0 D)$ becomes singular. This indicates that ordering will develop for an infinitesimal inducing field $h_{\beta}(\mathbf{q},\omega)$. The locus of such $(\mathbf{q},\omega)$ points provides the dispersion of collective excitations.

## III. A GENERIC INTERACTING WEYL SEMIMETAL

To develop a simple model for a Weyl semimetal, we consider the system shown in Fig. 1(a). At low energies, this system is described by a particularly simple single-particle Hamiltonian

$$\mathcal{H}^{\text{simp}}_{KE} = \sum_{\mathbf{k}} \Psi^{\dagger}_{\mathbf{k}} H_{\mathbf{k}} \Psi_{\mathbf{k}}, \tag{8}$$

where $\Psi^{\dagger}_{\mathbf{k}} = (c^{\dagger}_{c,L,\mathbf{k}}\ c^{\dagger}_{c,R,\mathbf{k}}\ c^{\dagger}_{v,L,\mathbf{k}}\ c^{\dagger}_{v,R,\mathbf{k}})$ is the array of quasiparticle creation operators. They are defined in the band basis with the index $c/v$ denoting conduction/valence bands. The $L/R$ indices represent the two valleys, with $\mathbf{k}$ representing deviation from the corresponding Weyl point. In this basis, the Hamiltonian matrix takes a simple form $H_{\mathbf{k}} = \text{Diag}\{+|\mathbf{k}|, +|\mathbf{k}|, -|\mathbf{k}|, -|\mathbf{k}|\}$. We set the Fermi velocity to unity and the chemical potential to zero, as appropriate for an isotropic undoped Weyl semimetal.

With the goal of developing a minimal model, we assume a simple form for interactions as shown in Figs. 2(b)–2(d). At low energies, two-particle processes can only be of two types: with low (comparable to zero) or high (comparable to $\mathbf{Q}$) momentum transfer. Low-momentum-transfer processes can be further subdivided into two classes: within a single valley or those involving both valleys. As a simplifying assumption, we take these processes to have momentum-independent amplitudes, given by $\alpha$, $\beta$, and $\gamma$ as shown in the figure. This

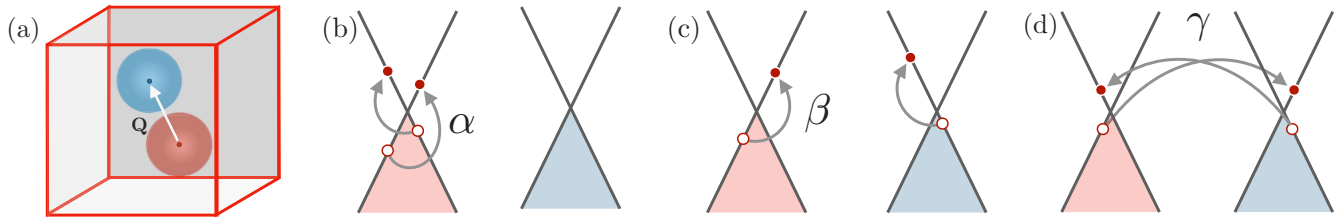


FIG. 2. (a) Brillouin zone for a three-dimensional lattice, assumed to be cubic for simplicity. The spherical regions around Weyl points show linear dispersion. We approximate the Brillouin zone as consisting only of these spherical regions. (b)–(d) Interaction processes at low energies. We have processes with small momentum transfer that involve the same valley ($\alpha$) or different valleys ($\beta$), apart from large-momentum-transfer intervalley scattering ($\gamma$).

leads to the Hamiltonian

$$\mathcal{H}_{\rm int}^{\rm simp} = \alpha \sum_{\eta=L,R} \sum_{\mathbf{k},\mathbf{k}',\mathbf{q}} c^\dagger_{c,\eta,\mathbf{k}+\mathbf{q}} c^\dagger_{c,\eta,\mathbf{k}'-\mathbf{q}} c_{v,\eta,\mathbf{k}'} c_{v,\eta,\mathbf{k}} + \beta \sum_{\mathbf{k},\mathbf{k}',\mathbf{q}} c^\dagger_{c,L,\mathbf{k}+\mathbf{q}} c^\dagger_{c,R,\mathbf{k}'-\mathbf{q}} c_{v,R,\mathbf{k}'} c_{v,L,\mathbf{k}} + \gamma \sum_{\mathbf{k},\mathbf{k}',\mathbf{q}} c^\dagger_{c,L,\mathbf{k}+\mathbf{q}} c^\dagger_{c,R,\mathbf{k}'-\mathbf{q}} c_{v,L,\mathbf{k}'} c_{v,R,\mathbf{k}}. \quad (9)$$

We neglect interaction terms involving $c_{c,L/R}$ or $c^\dagger_{v,L/R}$. Such terms will not enter the lowest-order (zero-temperature) susceptibility calculation described below. This form of the interaction Hamiltonian is admittedly simplistic. Nevertheless, it allows for an analytic calculation of the collective mode spectrum, which in turn brings out essential aspects of the problem.

### A. Evaluating bare susceptibility

We now apply the GRPA formalism taking the noninteracting Hamiltonian to be that in Eq. (8) and the interactions to be given by Eq. (9). The ordering tendencies in this system are represented by excitonic bilinears of the form $\hat{\rho}_{\eta\lambda}(\mathbf{q}) = \sum_{\mathbf{k}} c^\dagger_{c,\eta,\mathbf{k}+\mathbf{q}} c_{v,\lambda,\mathbf{k}}$, where $\eta, \lambda = L/R$ are valley indices. We organize these $\hat{\rho}_{\eta\lambda}$ operators into a vector, as in Eq. (1), to give

$$\hat{O}(\mathbf{q}) = (\hat{\rho}_{LL}(\mathbf{q})\ \hat{\rho}_{RR}(\mathbf{q})\ \hat{\rho}_{LR}(\mathbf{q})\ \hat{\rho}_{RL}(\mathbf{q})). \quad (10)$$

We do not consider pairing bilinears of the form $c_{c,\eta,-\mathbf{k}+\mathbf{q}} c_{v,\lambda,\mathbf{k}}$, as repulsive interactions are known to favor excitonic orders.

The bare susceptibility to these orders takes the Lindhard form

$$\chi^0_{(\ell_1\ell_2)(\ell_1'\ell_2')}(\mathbf{q},\omega) = \sum_{\mathbf{k}} \frac{\delta_{\ell_1\ell_1'}\delta_{\ell_2\ell_2'}}{(E_{\mathbf{k}+\mathbf{q}} + E_{\mathbf{k}} - \omega) + i0^+}, \quad (11)$$

where $E_{\mathbf{p}} = |\mathbf{p}|$ is the quasiparticle energy and $\ell$'s are valley indices. We have added an infinitesimal in the denominator for regularization. Since the bare susceptibility is diagonal in the $\hat{\rho}$ basis, we drop the indices and simply refer to it as $\chi^0(\mathbf{q},\omega)$. We evaluate this quantity assuming that (a) the Brillouin zone can be approximated as consisting of two spheres of radius $k_c$, each centered at a Weyl point, and (b) the linear dispersion around each Weyl point, as given in Eq. (8), extends over each entire sphere. These approximations can be justified by noting that the dominant contribution to the sum in Eq. (11) comes from the immediate neighborhood of each Weyl point; our approach indeed retains the correct quasiparticle energies here. In this picture, the particle-hole continuum has an intravalley and an intervalley component, both of which are bounded from below by the cone $\omega = |\mathbf{q}|$. The susceptibility is the same for both intravalley and intervalley sectors.

The susceptibility in Eq. (11) can be evaluated using an elegant geometric picture, by noting that $\mathrm{Im}(\chi^0(\mathbf{q},\omega))$ only receives contributions from $\mathbf{k}$ points which satisfy $E_{\mathbf{k}+\mathbf{q}} + E_{\mathbf{k}} = \omega$, i.e., $|\mathbf{k}+\mathbf{q}| + |\mathbf{k}| = \omega$. This relation describes an ellipsoid in $\mathbf{k}$ space with major axis along $\mathbf{q}$, as shown in Fig. 3. In fact, $\mathrm{Im}(\chi^0(\mathbf{q},\omega))$ simply counts the number of $\mathbf{k}$ points that lie on this surface. Details of the derivation are presented in Appendix A. We find

$$\mathrm{Im}(\chi^0(\mathbf{q},\omega)) \approx \begin{cases} \frac{\pi(3\omega^2 - q^2)}{6}, & q < \omega < (2k_c + q) \\ 0, & \text{otherwise} \end{cases} \quad (12)$$

which vanishes outside the particle-hole continuum. This quantity, near the bottom of the particle-hole continuum ($\omega \gtrsim q$), can be understood as the density of "free" particle-hole pairs that are available for exciton formation.

Remarkably, this expression reveals a quasi-two-dimensional character in the problem. As we approach the bottom of the particle-hole continuum from above ($\omega \to q^+$), we find that $\mathrm{Im}(\chi^0(\mathbf{q},\omega)) \to \pi q^2/3$, a constant for a given $\mathbf{q}$. This is analogous to the density of states of a conventional

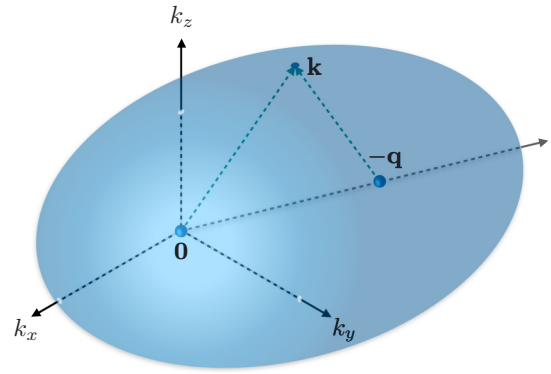


FIG. 3. Locus of points that contribute to $\mathrm{Im}(\chi^0(\mathbf{q},\omega))$, defined by $|\mathbf{k}| + |\mathbf{k}+\mathbf{q}| = \omega$. Any point on the surface has the sum of distances from the $\mathbf{0}$ and $-\mathbf{q}$ equal to $\omega$. These points form an ellipsoid in momentum space with foci at $\mathbf{0}$ and $-\mathbf{q}$. The major axis is along $\mathbf{q}$, with the semi-major axis being $\omega/2$. The eccentricity is given by $|\mathbf{q}|/\omega$.

two-dimensional metal. This indicates that exciton formation here is analogous to bound-state formation in a conventional two-dimensional system, even though we are concerned with a three-dimensional Weyl semimetal.

Using the Kramers-Kronig relation (see Appendix A), we obtain

$$\mathrm{Re}(\chi^0(\mathbf{q},\omega)) \approx \pi k_c^2 + \frac{\pi}{6}\left[12qk_c - 2q^2 \log\left\{\frac{q-\omega}{2k_c}\right\}\right]. \tag{13}$$

This expression holds near the upper boundary of the window in the particle-hole continuum ($\omega \lesssim q$). This is the region in $\omega - \mathbf{q}$ space that can develop collective excitations in the presence of weak interactions.

### B. Collective mode spectrum

Having found the bare susceptibility, we take interactions into account. The terms in Eq. (9) can be quadratically decomposed as

$$\mathcal{H}_{\mathrm{int}}^{\mathrm{simp}} \longrightarrow \sum_{\mathbf{q}} \langle \hat{O}(\mathbf{q})\rangle \cdot D^{\mathrm{simp}} \cdot \hat{O}^\dagger(\mathbf{q}), \tag{14}$$

where $\hat{O}$ has been defined in Eq. (10) and

$$D^{\mathrm{simp}} = \begin{bmatrix} \alpha & 2\beta & 0 & 0 \\ 2\beta & \alpha & 0 & 0 \\ 0 & 0 & 0 & 2\gamma \\ 0 & 0 & 2\gamma & 0 \end{bmatrix}. \tag{15}$$

The coefficients $\alpha$, $\beta$, and $\gamma$ are the interaction amplitudes described in Figs. 2(b)–2(d). Following the GRPA prescription, we obtain

$$\chi^{\mathrm{GRPA}}_{\alpha\beta,\eta\lambda}(\mathbf{q},\omega) = \{[1 - D^{\mathrm{simp}}\chi^0(\mathbf{q},\omega)]^{-1}\}_{\alpha\beta,\mu\zeta}\chi^0_{\mu\zeta,\eta\lambda}(\mathbf{q},\omega).$$

A collective mode emerges when $\chi^{\mathrm{GRPA}}(\mathbf{q},\omega)$ diverges. This occurs when $\det[1 - D^{\mathrm{simp}}\chi^0(\mathbf{q},\omega)] = 0$, leading to the following four solutions:

$$\omega_i = q - 2k_c \exp\frac{6(qk_c - t_i)}{q^2}, \quad i = 1,2,3,4 \tag{16}$$

where $t_i$ are given by

$$t_{1,2} = \frac{\frac{1}{\alpha\pm2\beta} - \pi k_c^2}{2\pi}, \quad t_{3,4} = \frac{\pm\frac{1}{2\gamma} - \pi k_c^2}{2\pi}. \tag{17}$$

These expressions come with the following caveat. They are derived from Eq. (13) which is only valid immediately below the particle-hole continuum, i.e., for $\omega \to q^-$. If they lead to a solution in this region of $\omega - q$ space, it represents a true collective mode. Solutions outside this region are spurious and not physically meaningful.

### C. Exciton binding energy

In the right-hand side of Eq. (16), the second term encodes binding energy of the collective mode, i.e., the separation from the bottom of the continuum. To have meaningful collective excitations as $\mathbf{q} \to 0$, at least one of the $t_i$'s must be positive. Otherwise, the binding energy grows without bound as $\mathbf{q}$ approaches zero. For example, if $\gamma > 0$ and $\gamma^{-1} \gg \pi k_c^2$, we see that $t_3$ is positive. This indicates that $\omega_3$ is a true collective mode as $\mathbf{q} \to 0$ with an exponentially small binding energy. If we now tune $\gamma$ to stronger values, the binding energy will increase and the collective mode will shift downwards. When $\gamma$ reaches a critical value $\gamma_c = (2\pi k_c^2)^{-1}$, $t_3$ vanishes. This indicates an instability of the Weyl semimetal to intervalley exciton condensation (as $\gamma$ is an intervalley process). Beyond this point, the binding energy grows sharply, indicating softening of the collective mode. More generally, the $t_i$'s in Eq. (17) encode critical interaction strengths at which instabilities arise.

We have argued above that exciton formation here is a problem of bound-state formation in effectively two dimensions. In this respect, it is directly analogous to the well-known Cooper pair [23] problem, e.g., as described in Ref. [24]. The two dimensionality arises as only a thin shell around the Fermi surface is considered. This leads to a constant density of states, $g(\epsilon_F)$. For weak interactions encoded by $V$, a bound state is formed with an exponentially small binding energy given by $E_{\mathrm{Cooper}} = 2\hbar\omega_D \exp[-2/g(\epsilon_F)V]$. This expression closely matches our result in Eq. (16). For concreteness, let us consider $i = 3$ with $\gamma > 0$ in the limit $q \to 0$. For weak interactions ($\gamma^{-1} \gg \pi k_c^2$), the binding energy comes out to be $E_b \approx 2k_c \exp(-3/2\pi q^2\gamma)$. This has precisely the same form as $E_{\mathrm{Cooper}}$; the $q^2$ in the exponent arises from the density of states of free particle-hole states [see $\mathrm{Im}(\chi^0(\mathbf{q},\omega))$ above].

We have demonstrated that excitons in Weyl semimetals are analogous to Cooper pairs in metals. The existence of bound Cooper pair solutions indicates an instability of the Fermi surface, showing that metals are generically unstable to superconductivity. Likewise, the particle-hole continuum in Weyl semimetals is unstable to exciton formation.

Our analysis here is based on a simple model with two Weyl points and momentum-independent interactions. We have implicitly assumed time-reversal breaking as this is a necessary condition for having only two Weyl points, e.g., see Ref. [25]. However, our reasoning is sufficiently general to apply to all Weyl semimetals with or without time-reversal breaking. In all these cases, with a suitable extension of Eq. (8), the bare susceptibility is the same as Eqs. (12) and (13) above. As a result, the argument for effective two dimensionality continues to hold. We conclude that all Weyl semimetals generically host undamped excitonic modes.

## IV. WEYL SEMIMETAL WITH THE HUBBARD INTERACTION

In the previous section, we have considered a minimal model of an interacting Weyl semimetal and derived analytic expressions for the collective mode spectrum. Here, we take a somewhat more realistic approach with a microscopically motivated Weyl Hamiltonian and onsite interactions. Following Burkov and Balents [26] (BB), we work with the noninteracting Hamiltonian

$$\mathcal{H}_{KE}^{\mathrm{BB}} = v_f(\hat{z}\times\boldsymbol{\sigma})\cdot\mathbf{k} + m(k_z)\sigma^z, \tag{18}$$

where $(\sigma^x,\sigma^y,\sigma^z)$ are the usual Pauli matrices and $m(k_z) = b - t(k_z)$, with $t(k_z) = \sqrt{t_S^2 + t_D^2 + 2t_S t_D\cos(k_z d)}$. This model was derived by considering a

topological-insulator–normal-insulator superlattice with broken time-reversal symmetry. The quantities $(t_S, t_D)$ represent effective hopping amplitudes in the heterostructure, while $b$ is the time-reversal-breaking term. It realizes a two-band model in which the two components of the wave function are the physical spin of the electron. The dispersion hosts Weyl points at momenta $(0, 0, P_{1,2})$, where

$$P_{1,2} = \pm\frac{\pi}{d} \mp \frac{1}{d}\cos^{-1}\left(\frac{t_S^2 + t_D^2 - b^2}{2t_S t_D}\right). \tag{19}$$

The length scale $d$ denotes the separation between layers. For later convenience, we define $\mathbf{Q} = (0, 0, P_1 - P_2)$, the vector separation between the two Weyl points. The low-energy excitations here are similar to the schematic in Figs. 1(a) and 1(b). In particular, the particle-hole continuum has two distinct low-energy regions: intravalley (momentum near zero) and intervalley (momentum near $\mathbf{Q}$).

We take the interaction Hamiltonian to be of the Hubbard form, given by

$$\mathcal{H}_{\text{int}}^{\text{Hubbard}} = \frac{U}{N}\sum_{\mathbf{k},\mathbf{k}',\mathbf{p}} c^\dagger_{\mathbf{k}+\mathbf{p},\uparrow} c^\dagger_{\mathbf{k}'-\mathbf{p},\downarrow} c_{\mathbf{k}',\downarrow} c_{\mathbf{k},\uparrow}. \tag{20}$$

The GRPA analysis of this problem takes different forms for intravalley ($\mathbf{q} \sim 0$) and intervalley sectors ($q \sim \mathbf{Q}$). In particular, the decomposition of the interaction is different in the two cases. We discuss these separately below.

### A. GRPA in the intervalley sector

Focusing on large momenta, low-energy excitations involve a particle from one valley and a hole from the other. To handle this structure, we divide the Brillouin zone into two regions. We label the $k_z > 0$ region as "right" ($R$) and $k_z < 0$ as "left" ($L$). The right and left valleys contain the Weyl points $(0, 0, P_1)$ and $(0, 0, P_2)$, respectively. We define creation/annihilation operators at low energies accordingly, e.g., $c^\dagger_{L,\mathbf{p},\sigma}$ denotes creation at momentum $\mathbf{p}$ lying below the $k_x$-$k_y$ plane. We consider bilinears of the form

$$\begin{aligned}\hat{\rho}_{\text{inter}}(\mathbf{q}) &= \frac{1}{2}\sum_{\mathbf{k}}\{c^\dagger_{R,\mathbf{k}+\mathbf{q},\uparrow} c_{L,\mathbf{k},\uparrow} + c^\dagger_{R,\mathbf{k}+\mathbf{q},\downarrow} c_{L,\mathbf{k},\downarrow}\},\\ \hat{S}^u_{\text{inter}}(\mathbf{q}) &= \frac{1}{2}\sum_{\mathbf{k},\mu,\mu'} c^\dagger_{R,\mathbf{k}+\mathbf{q},\mu}\sigma^u_{\mu,\mu'} c_{L,\mathbf{k},\mu'}.\end{aligned} \tag{21}$$

As we are interested in intervalley excitations, the net momentum $\mathbf{q}$ is restricted to values near $\mathbf{Q}$. The index $u = x, y, z$ denotes three possible spin directions. As in Eq. (1), we gather these bilinears into an array $\hat{O}_{\text{inter}}(\mathbf{q}) = [\hat{\rho}, \hat{S}^z_{\text{inter}}, \hat{S}^+_{\text{inter}}, \hat{S}^-_{\text{inter}}, \hat{\rho}^\dagger, \{\hat{S}^z_{\text{inter}}\}^\dagger, \{\hat{S}^+_{\text{inter}}\}^\dagger, \{\hat{S}^-_{\text{inter}}\}^\dagger]$. Here, $\hat{S}^\pm_{\text{inter}} = \hat{S}^x_{\text{inter}} \pm i\hat{S}^y_{\text{inter}}$.

Naively, we could have only considered spin-carrying bilinears $\hat{S}^u_{\text{inter}}(\mathbf{q})$ as repulsive interactions are known to favor spin-carrying collective modes. However, due to inherent spin-orbit coupling, there is no spin rotational symmetry in Eq. (18). As a consequence, at the level of bare susceptibility, $\hat{S}^u_{\text{inter}}(\mathbf{q})$ and $\hat{\rho}_{\text{inter}}(\mathbf{q})$ are mixed.

Decoupling the Hubbard interaction of Eq. (20) in terms of these bilinears, we obtain the coupling matrix $D^{\text{inter}}_{\alpha\beta} = \text{Diag}\{2, -2, -1, -1, 2, -2, -1, -1\}$ (details in Appendix B 1). We use these expressions in the GRPA formalism to find collective modes.

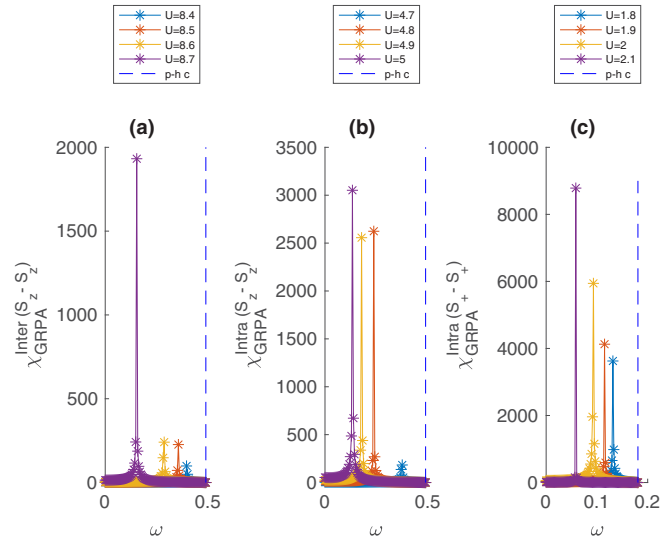


FIG. 4. Excitonic resonances manifested in spin-spin response calculated within GRPA. (a), (b) Intervalley and intravalley $\hat{S}_z$-$\hat{S}_z$ response as a function of frequency. The parameters used are $t_S = 1$, $t_D = 0.9$, $b = 1$, $v_f = 1$. (c) Intravalley $\hat{S}_+$-$\hat{S}_+$ response for $t_S = 1$, $t_D = 0.9$, $b = 1$, $v_f = 0.25$. In (a), the response is calculated at a momentum that is close to $\mathbf{Q}$. In (b) and (c), the momentum is close to zero. The dashed lines in each plot show the onset of the particle-hole continuum.

The bare susceptibility is an $8 \times 8$ matrix (see Appendix B 1 for explicit expressions). The elements of this matrix can only be found numerically. We evaluate them by discretizing the cubic Brillouin zone into a $L \times L \times L$ mesh, with $L$ up to 20. The singularities that occur at the Weyl point (the denominators in $\chi^0$ vanish here) are avoided by choosing parameters such that the Weyl points do not lie on the $\mathbf{k}$-mesh. An illustrative result is shown in Fig. 4(a). It plots the $\hat{S}^z_{\text{inter}} - \hat{S}^z_{\text{inter}}$ component of the $\chi^{\text{GRPA}}(\mathbf{q}, \omega)$ matrix vs $\omega$. The momentum $\mathbf{q}$ is kept fixed at a point in the vicinity of $\mathbf{Q}$. We see a clear divergent response, indicating a collective mode. This is brought about by one eigenvalue of $[1 + U\chi^0_{\text{inter}} D^{\text{inter}}]$ vanishing at this point. As shown in the figure, the collective mode shifts downwards as interaction $U$ is increased.

### B. GRPA in the intravalley sector

In the intravalley sector, we define bilinear operators

$$\begin{aligned}\hat{\rho}_{v=L/R}(\mathbf{q}) &= \frac{1}{2}\sum_{\mathbf{k}}\{c^\dagger_{v,\mathbf{k}+\mathbf{q},\uparrow} c_{v,\mathbf{k},\uparrow} + c^\dagger_{v,\mathbf{k}+\mathbf{q},\downarrow} c_{v,\mathbf{k},\downarrow}\},\\ \hat{S}^u_{v=L/R}(\mathbf{q}) &= \frac{1}{2}\sum_{\mathbf{k},\mu,\mu'} c^\dagger_{v,\mathbf{k}+\mathbf{q},\mu}\sigma^u_{\mu,\mu'} c_{v,\mathbf{k},\mu'}.\end{aligned} \tag{22}$$

The momentum $\mathbf{q}$ is taken to be small, with $|\mathbf{q}| \ll |\mathbf{Q}|$. The appropriate form of the bilinear array here is $\hat{O}_{\text{intra}}(\mathbf{q}) = [\hat{\rho}_L, \hat{S}^z_L, \hat{S}^+_L, \hat{S}^-_L, \hat{\rho}_R, \hat{S}^z_R, \hat{S}^+_R, \hat{S}^-_R]$. The Hubbard interaction can be decoupled in terms of this array with the coupling matrix $D^{\text{intra}}_{\alpha\beta} = \text{Diag}\{2, -2, -1, -1\} \otimes \left(\begin{smallmatrix}1 & 1\\ 1 & 1\end{smallmatrix}\right)$ (details in Appendix B 2). We evaluate $\chi^{\text{GRPA}}$ numerically as described in

Sec. IV A above. The resulting collective mode resonances are shown in Figs. 4(b) and 4(c). The plots show the $\hat{S}^z_L - \hat{S}^z_L$ and $\hat{S}^+_L - \hat{S}^+_L$ components of $\chi^{\text{GRPA}}$. The divergent peak indicates a collective mode which shifts downwards with increasing $U$.

## V. EXCITONS FROM HUBBARD INTERACTIONS

As discussed above, we find collective modes both in the intravalley and intervalley sectors. We elaborate on some aspects of the observed exciton modes below.

### A. Binding energy

Relatively large interaction strengths are required to see collective modes that are well separated from the continuum. In the intravalley sector, we see clear modes only for $U \gtrsim 5$ when $t_S$, $t_D$, $b$ are close to unity (bandwidth ∼4). In the intervalley sector, we require $U \gtrsim 8.5$. For comparison, the honeycomb lattice Hubbard model shows well-separated collective modes even for $U \sim 2$ when $t$ is unity (bandwidth ∼6) [27]. This can be understood from our analysis in Sec. III. The effective two-dimensional phase space of excitons leads to an exponentially small binding energy, thereby requiring a large interaction strength.

### B. Spin character

In both the intravalley and intervalley sectors, the collective modes carry spin. At resonant $(\mathbf{q}, \omega)$, we find large spin-spin components in the $\chi^{\text{GRPA}}_{\alpha\beta}(\mathbf{q}, \omega)$ matrix as shown in Fig. 4. In contrast, the density-density ($\hat{\rho}$-$\hat{\rho}$) components are negligible. We find two distinct collective modes: one with dominant $\hat{S}^z$ character and the other with $\hat{S}^\pm$ character. The latter is doubly degenerate, representing magnetic moment along $x$ and $y$ directions. In most regions of parameter space, only one of these modes is well separated from the continuum. Depending on $t_S$, $t_D$, $b$, and $v_F$, it is either the $\hat{S}^z$ mode or the $\hat{S}^\pm$ mode. Indeed, the anisotropy between $z$ and in-plane spin components is inherited from $\mathcal{H}^{\text{BB}}_{KE}$ in Eq. (18), which has different Fermi velocities in $z$ and in-plane directions.

### C. Exciton condensation

An exciting prospect in an interacting Weyl semimetal is the occurrence of an axionic insulator. In each valley, the Weyl semimetal Hamiltonian has a Clifford algebra structure with three Pauli matrices occurring in the Hamiltonian. At the level of a single valley, no perturbation can open a gap. However, taking both valleys together, there exists a mass term that opens a full gap. The resulting state is called the axionic insulator and has several interesting properties, including defects that carry gapless excitations [13]. As mass terms lead to large energy lowering by opening a full gap, one may expect that introducing interactions in a Weyl semimetal will lead to an axionic insulator. Such a transition has been argued to possess emergent supersymmetry with the collective modes and the electronic excitations acquiring the same group velocity [15]. Motivated by these arguments, we look for instabilities that arise from the Hubbard interaction. Within our GRPA approach, an instability will manifest as "softening" of a collective mode with its energy going to zero at some momentum $\mathbf{q}_{\text{inst}}$.

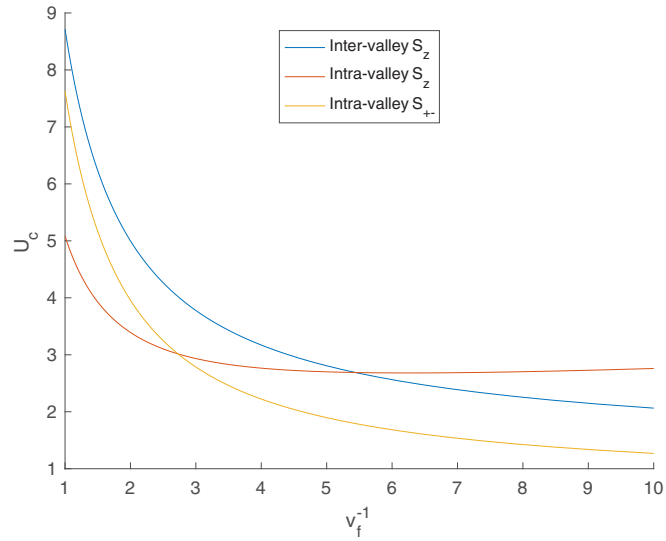


FIG. 5. Critical strengths ($U_c$) of intravalley and intervalley orderings at different values of $v_F^{-1}$. We have fixed $t_S = b = 1$ and $t_D = 0.9$. We do not show the intervalley $\hat{S}^\pm$ instability as it occurs at higher $U$ than the others.

Surprisingly, we find that the Hubbard interaction does not lead to an axionic insulator. As we increase $U$, we find that collective modes soften in the intravalley sector, at $\mathbf{q} = 0$. As the collective modes carry spin, we identify this as a magnetic instability. Depending on the parameters of $\mathcal{H}^{\text{BB}}_{KE}$, we find two regimes (we set $t_S = b = 1$ and $t_D = 0.9$ for concreteness): (a) for $v_F^{-1} < 2.8$, the leading instability is to spin ordering in the $z$ direction, and (b) for $v_F^{-1} > 2.8$, the leading instability is to ordering in the XY plane. This is shown in Fig. 5 which shows the critical interaction strength required for exciton condensation. The figure shows critical $U$ values for three different instabilities: (i) intravalley $\hat{S}^z$ ordering, (ii) intravalley $\hat{S}^\pm$ ordering, and (iii) intervalley $\hat{S}^z$ ordering. For each value of $v_F$, it is the smallest of these critical $U$'s that has physical significance. Beyond this $U_c$, the Weyl semimetal is unstable to magnetic order. We have independently confirmed these $U_c$ estimates by performing mean-field calculations for each magnetic order (intravalley $\hat{S}^z$, intravalley $\hat{S}^\pm$, and intervalley $\hat{S}^z$). In each case, a self-consistent magnetization emerges only when $U$ is increased beyond the corresponding critical value given by the GRPA analysis.

For any choice of parameters in $\mathcal{H}^{\text{BB}}_{KE}$, we find that the leading instability is always to intravalley ordering. This does not open a gap in the electron dispersion. Rather, it merely shifts the Weyl points. For example, when $v_f = 1$ in Fig. 5, the Weyl semimetal is stable until $U \approx 5.2$ where an excitonic mode with intravalley $\hat{S}^z$ character softens. This indicates that an axionic insulator does not emerge from Hubbard interactions.

## VI. SUMMARY AND DISCUSSION

We have discussed excitonic modes in Weyl semimetals. Our starting point is the observation of a window in the

particle-hole continuum that is conducive to the propagation of undamped collective modes. A similar window structure was pointed out by Baskaran and Jafari in the context of graphene. They argued that repulsive interactions in graphene naturally give rise to spin-1 (triplet) excitonic modes within this window. We have shown that these arguments extend to the three-dimensional case of Weyl semimetals. The window structure forbids the decay of collective excitations into particle-hole pairs. "Bosonic" damping is still possible via decay into pairs of collective excitations. However, this is a more subtle effect that we do not discuss here.

We have argued that Weyl semimetals have two-dimensional character from the point of view of collective mode formation. Low-energy particle-hole excitations lie on the surface of an ellipsoid in momentum space, constrained by linear single-particle dispersion and energy-momentum conservation. This effective two-dimensionality leads to an exponentially small binding energy. As a consequence, a large interaction strength is required to see excitons that are well separated from the particle-hole continuum.

In the context of graphene, the approach of Baskaran and Jafari in Refs. [6,7] was criticized [28] for not including sublattice character present in the microscopic description. In response, Baskaran and Jafari justified their approach by invoking an effective Fermi-liquid picture that is not necessarily microscopic [29]. Later on, Refs. [27,30] presented a GRPA analysis keeping the full microscopic structure of the honeycomb lattice Hubbard model. This does show the presence of excitonic modes. However, a critical interaction strength is required to have a well-defined linear mode at $\mathbf{q} \to 0$. (The analysis in Refs. [27,30] is presented in the language of the *attractive* Hubbard model. Nonetheless, these results also apply to the repulsive Hubbard model via a particle-hole transformation.) Beyond this critical value, the excitons condense to give rise to an antiferromagnet. In this antiferromagnetic phase, the collective modes split into Goldstone modes and an amplitude mode [27,31].

Our simplistic model, described in Sec. III, is analogous to the initial analysis of Baskaran and Jafari. It takes the single-valley Hamiltonian to be $\mathrm{Diag}\{|\mathbf{k}|, -|\mathbf{k}|\}$, rather than $\mathbf{k}\cdot\sigma$. As a consequence, it ignores the coherence factors that enter the eigenvectors of the single-particle Hamiltonian. Nevertheless, this analysis provides valuable insight by highlighting the effective two dimensionality of the phase space of particle-hole pairs. It shows that Weyl semimetals will generically host excitonic modes.

We go beyond this picture with a microscopic model in Sec. IV, providing a full GRPA treatment which clearly shows excitonic resonances. We find excitonic modes in both the intravalley and the intervalley sectors. We find that the intravalley excitons have a much larger binding energy. Upon increasing interaction strength, the excitons condense at zero momentum to give rise to a magnetic transition. The Weyl points merely shift without opening up a gap. Our results show that Hubbard-type interactions are unlikely to give rise to the axionic charge-density-wave (CDW) transition. This is consistent with results from cluster perturbation theory [8].

Throughout this paper, we have restricted our attention to the undoped Weyl semimetal with the chemical potential passing through the Weyl points. However, it can be readily seen that exciton modes will survive for small doping. The window in the particle-hole continuum survives partially when the chemical potential is shifted, as shown in Ref. [32] for graphene. By continuity arguments, exciton modes will survive within what remains of the window.

Our study of charge-neutral spin-carrying exciton modes serves a counterpoint to earlier work on charged plasmonic collective modes in Weyl semimetals [33–38]. Our analysis in Secs. IV and V, in a time-reversal-breaking Weyl semimetal, brings out the role of spin-orbit coupling in collective excitations. This bears parallels with earlier work on collective modes in topological insulator surfaces [39,40] and in metals with spin-orbit coupling [41].

Excitonic modes have been experimentally seen in several graphenelike systems [42–47]. Other two-dimensional systems with a Dirac-type low-energy description, transition metal dichalcogenides in particular, also host excitonic modes [48–50]. Our study shows that three-dimensional Dirac systems are also highly conducive to exciton formation. In particular, probes such as neutron scattering and photoabsorption could reveal excitonic resonances in candidate Weyl materials.

## ACKNOWLEDGMENTS

We thank G. Baskaran and S. A. Jafari for insightful discussions and comments. N.S.S. thanks S. Khatua and P. Raman for discussions.

## APPENDIX A: EVALUATING BARE SUSCEPTIBILITY

The sum in Eq. (11) can be converted into an integral. In particular, the imaginary part of $\chi^0(\mathbf{q},\omega)$ only receives contributions from points where the real part of the denominator vanishes. More precisely, $\chi^0(\mathbf{q},\omega)$ counts the number of $\mathbf{k}$ points that satisfy $E_{\mathbf{k}+\mathbf{q}} + E_{\mathbf{k}} = \omega$. This leads to

$$\mathrm{Im}(\chi^0(\mathbf{q},\omega)) = \int_{|k|<k_c} d^3k \;\; \delta[\omega - (E_{\mathbf{k}+\mathbf{q}} + E_{\mathbf{k}})]. \quad \text{(A1)}$$

To evaluate this, we consider a potential function $f_{\mathbf{q}}(\mathbf{k}) = E_{\mathbf{k}+\mathbf{q}} + E_{\mathbf{k}}$. The delta function picks out an equipotential surface on which $f_{\mathbf{q}}$ takes the value $\omega$. This integral can be evaluated using methods that are typically used in density-of-states calculations

$$\mathrm{Im}(\chi^0(\mathbf{q},\omega)) = \int_{\mathcal{E}} \frac{ds}{|\nabla_k f_{\mathbf{q}}(\mathbf{k})|}, \quad \text{(A2)}$$

where $\mathcal{E}$ denotes the equipotential surface in $\mathbf{k}$ space where $f_{\mathbf{q}} = \omega$, with $ds$ being its area element. The magnitude of the gradient in the denominator gives the density of states that are available in the vicinity of the point on the surface. As described in the main text, this surface is an ellipsoid.

We evaluate this integral in spherical coordinates. Taking $\mathbf{q}$ to lie along the $z$ direction, we define polar and azimuthal angles $\theta$ and $\phi$. The condition $\{f_{\mathbf{q}} = \omega\}$ reduces to $\{k + \sqrt{k^2+q^2+2kq\cos\theta} = \omega\}$, which determines $k$ as a function of $\theta$. We obtain $k_\theta = \frac{\omega^2-q^2}{2(\omega+q\cos\theta)}$. The integral becomes

$$\int_0^{2\pi} d\phi \int_0^{\pi} k_\theta \sin\theta \sqrt{k_\theta^2 d\theta^2 + dk_\theta^2} \frac{\omega^2+q^2+2\omega q\cos\theta}{2(\omega+q\cos\theta)} = \frac{\pi(3\omega^2-q^2)}{6}, \quad q < \omega < (2k_c+q). \quad \text{(A3)}$$

If $\omega$ were to be less than $q$ or greater than $2k_c + q$, then $\mathrm{Im}(\chi^0_{\alpha\beta}(\mathbf{q}, \omega))$ vanishes. The real part of the susceptibility can be evaluated using the Kramers-Kronig relation

$$\begin{aligned}&\mathrm{Re}(\chi^0(\mathbf{q}, \omega))\\ &= \pi k_c^2 + \frac{\pi}{6}\Bigg[6(q+\omega)k_c + (q^2 - 3\omega^2)\\ &\quad\times \log\left\{\frac{q-\omega}{2k_c+q-\omega}\right\}\Bigg], \quad \omega < q. \end{aligned} \tag{A4}$$

Close to the particle-hole continuum ($\omega \lesssim q$), the above expression can be approximated as

$$\mathrm{Re}(\chi^0(\mathbf{q}, \omega)) = \pi k_c^2 + \frac{\pi}{6}\left[12qk_c - 2q^2 \log\left\{\frac{q-\omega}{2k_c}\right\}\right]. \tag{A5}$$

## APPENDIX B: GRPA EXPRESSIONS

To evaluate the bare susceptibility matrix, we first diagonalize the noninteracting Hamiltonian of Eq. (18). This is achieved by a unitary transformation $\gamma_{\mathbf{k},v} \equiv U_{v,\sigma}(\mathbf{k})c_{\mathbf{k},\sigma}$. Here, $\gamma$'s are quasiparticle operators in the band basis and $U(\mathbf{k})$ is $2 \times 2$ unitary matrix. The diagonalized Hamiltonian is $\mathrm{Diag}\{E_{\mathbf{k}}, -E_{\mathbf{k}}\}$ where $E_{\mathbf{k}} = \sqrt{k_x^2 + k_y^2 + m(k_z)^2}$.

As described in the main text, we identify suitable bilinears for the intervalley and intravalley sectors separately. The expressions for the bare susceptibility matrix are given below.

### 1. Intervalley

In the intervalley sector, the bare susceptibility is given by the expression

$$\chi^0_{\mu\nu}(\mathbf{q}, \omega) = \frac{1}{N}\sum_{\mathbf{k}\in L}\left[\frac{M^\mu(\mathbf{k}, \mathbf{q})[M^\nu(\mathbf{k}, \mathbf{q})]^*}{\omega + E(\mathbf{k}+\mathbf{q}) + E(\mathbf{k})} - \frac{N^\nu(\mathbf{k}, \mathbf{q})[N^\mu(\mathbf{k}, \mathbf{q})]^*}{\omega - E(\mathbf{k}+\mathbf{q}) - E(\mathbf{k})}\right]. \tag{B1}$$

Here, the momentum $\mathbf{k}$ is summed over the left half of the Brillouin zone ($k_z < 0$) to avoid double counting. The momentum $\mathbf{q}$ is restricted to the vicinity of $\mathbf{Q}$ so that we only consider intervalley excitations. The indices $\mu$ and $\nu$ denote components of the vector of bilinears defined in the main text. The nonzero elements of $\chi^0$ are obtained by plugging the following functions into Eq. (B1):

$$\begin{aligned} M^{\hat{\rho}/\hat{S}_z} &= \tfrac{1}{2}[U^*_{12}(\mathbf{k}+\mathbf{q})U_{11}(\mathbf{k}) \pm U^*_{22}(\mathbf{k}+\mathbf{q})U_{21}(\mathbf{k})]\\ &= N^{\hat{\rho}^\dagger/\hat{S}_z{}^\dagger},\\ M^{\hat{\rho}^\dagger/\hat{S}_z{}^\dagger} &= \tfrac{1}{2}[U_{11}(\mathbf{k}+\mathbf{q})U^*_{12}(\mathbf{k}) \pm U_{21}(\mathbf{k}+\mathbf{q})U^*_{22}(\mathbf{k})]\\ &= N^{\hat{\rho}/\hat{S}_z},\\ M^{\hat{S}^+} &= U^*_{12}(\mathbf{k}+\mathbf{q})U_{21}(\mathbf{k}) = N^{(\hat{S}^+)^\dagger},\\ M^{\hat{S}^-} &= U^*_{22}(\mathbf{k}+\mathbf{q})U_{11}(\mathbf{k}) = N^{(\hat{S}^-)^\dagger},\\ M^{(\hat{S}^+)^\dagger} &= U^*_{22}(\mathbf{k})U_{11}(\mathbf{k}+\mathbf{q}) = N^{\hat{S}^+},\\ M^{(\hat{S}^-)^\dagger} &= U^*_{12}(\mathbf{k})U_{21}(\mathbf{k}+\mathbf{q}) = N^{\hat{S}^-}. \end{aligned} \tag{B2}$$

### 2. Intravalley

We use the eight-component vector of intravalley bilinears as defined in the main text. The first four elements correspond to the left valley while the next four correspond to the right valley. The bare susceptibility matrix takes the form

$$\chi^0_{\mu\nu}(\mathbf{q}, \omega) = \begin{pmatrix} \chi^L_{\mu\nu}(\mathbf{q}, \omega) & 0_{4\times4} \\ 0_{4\times4} & \chi^R_{\mu\nu}(\mathbf{q}, \omega)\end{pmatrix}. \tag{B3}$$

It is block diagonal in the valley basis as perturbations within one valley cannot induce a response in the other. The valley susceptibilites are given by

$$\chi^{L/R}_{\mu\nu}(\mathbf{q}, \omega) = \frac{1}{N}\sum_{\mathbf{k}\in L/R}\left[\frac{M^\mu(\mathbf{k}, \mathbf{q})[M^\nu(\mathbf{k}, \mathbf{q})]^*}{\omega + E(\mathbf{k}+\mathbf{q}) + E(\mathbf{k})} - \frac{N^\nu(\mathbf{k}, \mathbf{q})[N^\mu(\mathbf{k}, \mathbf{q})]^*}{\omega - E(\mathbf{k}+\mathbf{q}) - E(\mathbf{k})}\right]. \tag{B4}$$

For each valley, $\mathbf{k}$ is summed over the corresponding region ($k_z < 0$ or $k_z > 0$). The momentum $\mathbf{q}$ is restricted to the vicinity of zero to ensure that we have intravalley excitations. The functions in Eq. (B4) are given by

$$\begin{aligned} M^{\hat{\rho}/\hat{S}^z} &= \tfrac{1}{2}[U^*_{12}(\mathbf{k}+\mathbf{q})U_{11}(\mathbf{k}) \pm U^*_{22}(\mathbf{k}+\mathbf{q})U_{21}(\mathbf{k})],\\ M^{\hat{S}^+} &= U^*_{12}(\mathbf{k}+\mathbf{q})U_{21}(\mathbf{k}), \quad M^{\hat{S}^-} = U^*_{22}(\mathbf{k}+\mathbf{q})U_{11}(\mathbf{k}),\\ N^{\hat{\rho}/\hat{S}^z} &= \tfrac{1}{2}[U^*_{12}(\mathbf{k})U_{11}(\mathbf{k}+\mathbf{q}) \pm U^*_{22}(\mathbf{k})U_{21}(\mathbf{k}+\mathbf{q})],\\ N^{\hat{S}^+} &= U^*_{22}(\mathbf{k})U_{11}(\mathbf{k}+\mathbf{q}),\\ N^{\hat{S}^-} &= U^*_{12}(\mathbf{k})U_{21}(\mathbf{k}+\mathbf{q}). \end{aligned} \tag{B5}$$

In each function, the momentum argument determines if it is evaluated in the left or right region.


[1] A. H. Castro Neto, F. Guinea, N. M. R. Peres, K. S. Novoselov, and A. K. Geim, Rev. Mod. Phys. **81**, 109 (2009).
[2] S. Rao, J. Indian Inst. Sci. **96**, 145 (2016).
[3] B. Yan and C. Felser, Annu. Rev. Condens. Matter Phys. **8**, 337 (2017).
[4] N. P. Armitage, E. J. Mele, and A. Vishwanath, Rev. Mod. Phys. **90**, 015001 (2018).
[5] V. N. Kotov, B. Uchoa, V. M. Pereira, F. Guinea, and A. H. Castro Neto, Rev. Mod. Phys. **84**, 1067 (2012).
[6] G. Baskaran and S. A. Jafari, Phys. Rev. Lett. **89**, 016402 (2002).
[7] S. A. Jafari and G. Baskaran, Eur. Phys. J. B **43**, 175 (2005).
[8] W. Witczak-Krempa, M. Knap, and D. Abanin, Phys. Rev. Lett. **113**, 136402 (2014).

[9] B. Roy, P. Goswami, and V. Juričić, Phys. Rev. B **95**, 201102 (2017).
[10] J. Maciejko and R. Nandkishore, Phys. Rev. B **90**, 035126 (2014).
[11] S. Sorella, Y. Otsuka, and S. Yunoki, Sci. Rep. **2**, 992 (2012).
[12] B. Roy and J. D. Sau, Phys. Rev. B **92**, 125141 (2015).
[13] Z. Wang and S.-C. Zhang, Phys. Rev. B **87**, 161107 (2013).
[14] J. Wang, B. Lian, and S.-C. Zhang, Phys. Rev. B **93**, 045115 (2016).
[15] S.-K. Jian, Y.-F. Jiang, and H. Yao, Phys. Rev. Lett. **114**, 237001 (2015).
[16] G. Ramachandran, Competing orders in strongly correlated systems, Ph.D. thesis, University of Toronto, 2011, Chap 5.
[17] Y. Yunomae, D. Yamamoto, I. Danshita, N. Yokoshi, and S. Tsuchiya, Phys. Rev. A **80**, 063627 (2009).
[18] R. Ganesh, A. Paramekanti, and A. A. Burkov, Phys. Rev. A **80**, 043612 (2009).
[19] C.-M. Liegener, Phys. Lett. A **85**, 324 (1981).
[20] Z. G. Koinov, M. Fortes, M. de Llano, and M. A. Solís, Phys. Status Solidi B **247**, 2207 (2010).
[21] D. J. Rowe, Rev. Mod. Phys. **40**, 153 (1968).
[22] L. Belkhir and M. Randeria, Phys. Rev. B **49**, 6829 (1994).
[23] L. N. Cooper, Phys. Rev. **104**, 1189 (1956).
[24] C. Esebbag, J. M. Getino, M. de Llano, S. A. Moszkowski, U. Oseguera, A. Plastino, and H. Rubio, J. Math. Phys. **33**, 1221 (1992).
[25] I. Belopolski, P. Yu, D. S. Sanchez, Y. Ishida, T.-R. Chang, S. S. Zhang, S.-Y. Xu, H. Zheng, G. Chang, G. Bian, H.-T. Jeng, T. Kondo, H. Lin, Z. Liu, S. Shin, and M. Z. Hasan, Nat. Commun. **8**, 942 (2017).
[26] A. A. Burkov and L. Balents, Phys. Rev. Lett. **107**, 127205 (2011).
[27] S. Tsuchiya, R. Ganesh, and T. Nikuni, Phys. Rev. B **88**, 014527 (2013).
[28] N. M. R. Peres, M. A. N. Araújo, and A. H. Castro Neto, Phys. Rev. Lett. **92**, 199701 (2004).
[29] G. Baskaran and S. A. Jafari, Phys. Rev. Lett. **92**, 199702 (2004).
[30] S. Tsuchiya, R. Ganesh, and A. Paramekanti, Phys. Rev. A **86**, 033604 (2012).
[31] M. Lu, H. Liu, P. Wang, and X. C. Xie, Phys. Rev. B **93**, 064516 (2016).
[32] M. Ebrahimkhas, S. A. Jafari, and G. Baskaran, Int. J. Mod. Phys. B **26**, 1242006 (2012).
[33] S. Ahn, E. H. Hwang, and H. Min, Sci. Rep. **6**, 34023 (2016).
[34] J. Hofmann and S. Das Sarma, Phys. Rev. B **93**, 241402 (2016).
[35] J. C. W. Song and M. S. Rudner, Phys. Rev. B **96**, 205443 (2017).
[36] J. Hofmann and S. Das Sarma, Phys. Rev. B **91**, 241108 (2015).
[37] M. D. Redell, S. Mukherjee, and W.-C. Lee, Phys. Rev. B **93**, 241201 (2016).
[38] J. Zhou, H.-R. Chang, and D. Xiao, Phys. Rev. B **91**, 035114 (2015).
[39] J.-H. Jiang and S. Wu, Phys. Rev. B **83**, 205124 (2011).
[40] H.-H. Kung, S. Maiti, X. Wang, S.-W. Cheong, D. L. Maslov, and G. Blumberg, Phys. Rev. Lett. **119**, 136802 (2017).
[41] S. Maiti, V. Zyuzin, and D. L. Maslov, Phys. Rev. B **91**, 035106 (2015).
[42] F. Wang, G. Dukovic, L. E. Brus, and T. F. Heinz, Science **308**, 838 (2005).
[43] Y.-Z. Ma, L. Valkunas, S. M. Bachilo, and G. R. Fleming, J. Phys. Chem. B **109**, 15671 (2005).
[44] M. S. Dresselhaus, G. Dresselhaus, R. Saito, and A. Jorio, Annu. Rev. Phys. Chem. **58**, 719 (2007).
[45] J. Shinar, *Optical and Electronic Properties of Fullerenes and Fullerene-Based Materials*, edited by J. Shinar, Z. V. Vardeny, and Z. H. Kafafi (Marcel Dekker, New York, 1999).
[46] L. Yang, M. L. Cohen, and S. G. Louie, Nano Lett. **7**, 3112 (2007).
[47] P. Yadav and S. Ghosh, in *Proceedings of the 59th DAE Solid State Physics Symposium 2014*, edited by D. Bhattacharyya, R. Chitra, and N. K. Sahoo, AIP Conf. Proc. No. 1665 (AIP, New york, 2015), p. 050075.
[48] A. Singha, M. Gibertini, B. Karmakar, S. Yuan, M. Polini, G. Vignale, M. I. Katsnelson, A. Pinczuk, L. N. Pfeiffer, K. W. West, and V. Pellegrini, Science **332**, 1176 (2011).
[49] Y. Park, Y. Kim, C. W. Myung, R. A. Taylor, C. C. S. Chan, B. P. L. Reid, T. J. Puchtler, R. J. Nicholas, L. T. Singh, G. Lee, C.-C. Hwang, C.-Y. Park, and K. S. Kim, ACS Nano **11**, 3207 (2017).
[50] K. S. Thygesen, 2D Mater. **4**, 022004 (2017).